ICANS IX

INTERNATIONAL COLLABORATION ON ADVANCED NEUTRON SOURCES

22-26 September, 1986

EXPERIMENTAL AND THEORETICAL ANALYSIS OF THE HIGH ENERGY DEEP PENETRATION EXPERIMENT AT WNR - LOS ALAMOS (KFA/IRE - LANL/P9 COLLABORATION)

W.B. Amian, H. Schaal, V. Drüke, P. Cloth, D. Filges and N. Paul
Institut für Reaktorentwicklung, Kernforschungsanlage Jülich
Postfach 1913, D-5170 Jülich Germany

I. INTRODUCTION

In this paper a deep penetration experiment conducted at the Los Alamos WNR facility's Spallation Neutron Target /1/ is compared with calculations using the HETC/KFA-1 /2/, and ANISN /3/ codes installed at KFA-IRE.

For such problems the most reasonable technique to detect neutrons experimentally is by counting decaying residual nuclei of high energy interactions with suitable target materials. Especially for accelerator environments, spallation reactions on copper have been proposed by Routti /4/ as a means to extend the known threshold-foil technique to higher hadron energies. The yield cross sections for many spallation products have a threshold type energy dependence with threshold energies of tens or hundreds of MeV.

The problem with these reactions, however, is that the spallation yield cross sections are basically not known above 20 MeV. While the experiments can reveal clearly the exponential decrease of reaction rates with shielding thickness without any prior knowledge of cross sections, the quantitative comparison

between experiment and calculation suffers from the lack of reliable cross section data for these spallation yield cross sections.

We will demonstrate this deficiency by a comparison of experimental and theoretically determined production cross sections for some isotopes from natural copper. For more detailed information see Ref. /5/.

II. EXPERIMENTAL

Foils of 30 mm diameter and 1 mm thickness were irradiated inside the WNR target 1 bulk shield. They were imbedded into a stringer assembly that was inserted into flight path 5 of the facility. Foil materials studied were copper, cobalt, and nickel, all of natural isotopic composition. The stringer assembly loaded with iron foil containers and part of the WNR bulk shield are shown in Figure 1 and Figure 2, respectively.

During irradiations, ^{3}He-detector counts were recorded to correct for time variations of the proton-beam intensity and the resulting neutron-flux intensity. The ^{3}He detector was positioned in a polyethylene cylinder at the flight path's end (Fig. 1). This position was chosen to prevent interference from neighbouring experiments. The irradiations were performed with a tungsten target (4.45 cm diameter, 24 cm length) and a beryllium reflected water moderator assembly in place. Typical proton beam currents were approximately 3 μA.

After irradiations the reaction products in all foils were determined directly by counting in Ge(Li) gamma-ray spectrometers. All foil activities were corrected for self absorption in the foils, for decay during irradiation utilizing the recorded ^{3}He-detector counts, and for decay during counting. They

are for the time at the end of bombardment. The final reaction rates are normalized to the number of primary protons interacting in the target and the number of foil nuclei.

These reaction rates have been multiplied by the distance to the target squared and have been plotted versus depth in the shield. Results for some spallation reactions on copper are shown in Fig. 3 and 4.

III. HETC AND ANISN CALCULATIONS

Combined Monte Carlo and deterministic transport calculations were performed for the experimental arrangement of Fig. 2 to calculate the reaction rates for the measured reactions on copper. Two important simplifications can be done due to the fact that nearly all reactions used in the experiments have threshold energies above 15 MeV:

1. It is not necessary to follow neutrons in energy below 15 MeV, i.e. it is adequate to use only the Monte Carlo code HET/KFA-1 /2/ with a cut-off energy at 15 MeV and neglect subsequent low enery transport calculations.
2. It is allowed to simplify the complex moderator-reflector system surrounding the target (see Fig. 2) and simply describe it as a homogeneous beryllium cylinder, because in the shielding context the entire system is of interest only for removing high energy particles. The low energy particles stemming from moderations will not be measured by the threshold detectors and can therefore be neglected in the shielding calculations.

This simplifies our shielding calculation as compared to target calculations considerably.

Calculational Procedure

The particle histories were calculated with HET/KFA-1 down to the lower energy limit of 15 MeV. The histories were started by incoming protons of 800 MeV hitting the top surface of the cylindrical tungsten target (Fig. 5). The particle fluxes inside the shield were determined in two different ways:

1. Straight forward Monte Carlo with HETC and SIMPEL analysis. The code SIMPEL of the system /2/ derived neutron fluxes and proton fluxes at different depths inside the shield using track-length estimators.
2. HETC-ANISN surface coupling procedure via SIMPEL. Close to the inner surface of the bulk shield a spherical segment was defined serving as a coupling surface between SIMPEL and ANISN /3/. Here SIMPEL calculated a neutron surface source, which was handed over to the one-dimensional transport code ANISN. Starting with this source, ANISN calculated the neutron fluxes inside the shield in spherical geometry. The coupling procedure is described in /5/. The transport cross sections used for the calculations were taken from the LANL library /6/.

Both HETC and HETC-ANISN coupling calculated fluxes were folded with corresponding reaction cross sections to obtain reaction rates. Two sets of cross sections were generated using the RUDSTAM formulas /7/ and the code ALICE /8/, respectively.

Geometry

The geometrical layout for the HETC calculations was described using concentrical cylinders (see Fig. 5) with the following zones and materials:

Zone 1 was the tungsten target, zone 2 the beryllium reflector - the simplifying assumption for the moderator-reflector system. The radius of this reflector was set to the actual thickness in the line of sight in the experimental arrangement for FP5 from the target center to the surface of the stringer. Zone 3 is a void region and zone 4 is the shield which consists of a mixture of iron and concrete.

For the flux estimation from HETC histories SIMPEL used track length estimators which were rings of 20 cm heights and thicknesses of about 3 cm. These volume detectors are denoted A, B, C in Fig. 5. The advantage of such ring shaped detectors is the strongly enhanced statistics due to the azimuthal symmetry as compared to small detector boxes.

The coupling surface of the neutron surface source used by ANISN (denoted SQ in Fig. 5) was a spherical segment with radius 122 cm. This segment was placed entirely into the bulk shield. This geometry is not azimuthal symmetric. For the ANISN transport calculations beyond the coupling surface the bulk shield was assumed to be composed of iron only with nuclide density 8.44×10^{22} cm^{-3}. This is assumed to be the better approximation to the environment of the monitor foils inside the stringer than the iron/concrete mixture of the bulk shield.

IV. RESULTS

HETC and the HETC-ANISN coupling calculate particle fluxes for energies between 800 MeV and 15 MeV at different depths inside the shield. The proton flux is negligable as compared to the neutron flux as Table I shows. Therefore, protons have been neglected in all calculations following. Looking at the depth dependence in Table I, a comparison of the HETC-ANISN coupling and HETC results shows, that the high energy flux as calculated

by HETC is not decreasing as fast as predicted by the HETC-ANISN coupling while going further into the shield. The reason for this behaviour could be that for the HETC calculation a mixture of iron and concrete with an iron number density of 7.7×10^{22} cm^{-3} was assumed, while for the coupling calculation pure iron with a number density of 8.44×10^{22} cm^{-3} was used to account for the true material composition inside the stringer.

Flux Spectra

Fig. 6 shows a comparison of the flux spectra calculated by HETC at two different depths inside the shield. At 23 cm the spectrum is harder than at 103 cm depth. The reason could be that the mixture of iron and concrete acts as a moderator. But it should be mentioned that at 103 cm depth the fractional standard deviation values (FSD) for all energy groups of the spectrum are in the range of about 50 percent, indicating bad statistics. To compare the predictions of the spectral behaviour of both procedures the spectrum calculated by the HETC-ANISN coupling and the HETC spectrum are plotted in Fig. 7 at 23 cm depth. We have chosen this position because it is close to the coupling surface SQ in Fig. 5 and good statistics can be obtained with HETC itself. As expected, good agreement between both spectra is obtained. Fig. 8 gives the spectra calculated by the HETC-ANISN coupling at three different depth

In contrast to the spectrum behaviour calculated by HETC (Fig.6), the HETC-ANISN coupling spectrum is harder at 103 cm than at 23 cm depth. Furthermore, Fig. 8 shows that the spectra at 103 cm depth and in 203 cm are nearly identical. Therefore, it can be stated that the HETC-ANISN coupling spectra reach equilibrium very fast.

Reaction Rates

Calculated results that can be compared with the experiments are the threshold reaction rates. They were calculated by folding the group dependent neutron fluxes with reaction cross sections. Reaction rates were generated for two positions at 23 cm and 103 cm. In Table II the calculated and measured rates for the reactions on foils of natural copper are shown. Agreement within a factor of two between measured and calculated reaction rates is found for the Rudstam cross sections. It should be mentioned, however, that both the measured reaction rates and the calculated fluxes contain uncertainties of up to 50 percent (see spectrum results in Figs. 6-8). Much larger differences between measurement and calculation up to more than a factor of 10 are found if reaction cross sections generated by the code ALICE /8/ are used to calculate the reaction rates.

V. DISCUSSION

In comparing experiment and calculation the most serious source of uncertainty are the neutron cross sections for the production of residual nuclei in the monitor foils. It is simplistically assumed that at high energies (above 20 MeV) spallation cross sections for protons and neutrons are identical. The common description of this process as an intranuclear cascade and a subsequent evaporation process is in favour of this ide equal response to both nucleons. Therefore, cross sections for proton induced reactions which are much easier to obtain experimentally than neutron cross sections were compiled and treated like neutron cross sections to calculate the reaction rates at different positions in the shield. Sources of cross sections were the Rudstam /7/ formulas, which are semiempirical parameterizations of experimental results up to 1964, the modifications by Silberberg and Tsao /9/, more recent experiments on

copper targets reported by Orth /10/, Grüttner /11/, Williams /12/ and Greenwood /13/ and, finally, preequilibrium calculations with ALICE /8/.

For one example part of the compilations is shown in Fig. 9. The Silberberg/Tsao cross sections were not included in the plots because their general shape follows Rudstam's curves with up to 50% deviation to both sides. In Fig. 9 the agreement between experiments and ALICE calculations for the production of ^{57}Co from copper is reasonable close to the threshold energy. At higher energies they disagree significantly with ALICE predicting a steep decrease. Rudstam's curve is systematically too low, Silberberg/Tsao's prediction would hit the last point of Greenwood's experiment. The resulting large difference between the reaction rates calculated from both Rudstam's and ALICE's cross sections is found in Table II for ^{57}Co. The experimental reaction rate in Table II should be closer to the reaction rate obtained by folding the calculated neutron flux with ALICE's cross sections. But these cross sections seem to be the upper limits as compared to the more recent experimental cross sections.

The discussion shows that we can only argue within factors of two or three or more from these monitor reaction cross sections alone. The total disagreement between ALICE's and Rudstam's (or Silberberg/Tsao's) cross sections and experimental values makes any evaluation effort obsolete. ALICE seems to follow the general shape of the experimental results better than the Rudstam formulas, but still with large discrepancies. Under this aspect there is a strong need for cross section measurements especially above 70 MeV to produce a reliable data base. Not until cross sections have been obtained with reasonable uncertainties (of at least better than a factor of 2) and sufficiently narrow energy spacings at the threshold energies, more accurate comparisons between experiment and calculations cannot be expected.

VI. CONCLUSION

The deep penetration experiment at the WNR helped to generate an experimental data base for a well defined spallation physics environment to be compared with predictions of the HETC/KFA-1, SIMPEL and ANISN codes. The experiment's position perpendicular to the beam axis excluded primary protons and most of the high-energy neutrons beyond the evaporation neutron energies. This made especially the HETC calculations more elaborate, because most of the histories are in forward direction or are confined within the target/reflector volume. To get enough statistics perpendicular to the beam axis 122 cm away from the target calls certainly for more CPU time, but without making all simplifying assumptions and taking full advantage of the approximate symmetry of the WNR target, CPU time would be unreasonably large.

The direct comparison between experiment and calculation was based on the measured reaction rates, any unfolding of the experimental data would have introduced additional sources of uncertainty beyond cross sections. The agreement is not too satisfactory, but as the compilation of reaction cross sections for natural copper targets shows, cross sections for the production of nuclei in the detector foils alone are the largest source of uncertainty, larger than Monte Carlo statistics, coupling between codes or proton contributions. The results presented show that experiment and both HETC and ANISN calculations do compare to some extent, but the overall uncertainties introduced by the cross section for the specific reaction excludes conclusions as to how to improve the calculational model.

Basically one has to conclude that cross sections for the detection reactions studied have to be measured first with reasonable accuracy to provide a reliable base for comparing experiment and calculation. The lack of experimental cross sections above 20 MeV is certainly due to the fact that accelerators with variable particle energies between 1 GeV and 20 MeV are not available. The proposed COSY synchrotron that will produce protons between 2.5 GeV and 40 MeV would be the ideal facility to measure the required cross sections.

VII. REFERENCES

/1/ W. Amian, V. Drüke, N. Paul, G.J. Russell, P. Cloth, Dr. Filges, H. Schaal
Experiments and Theoretical Investigations for a High-Energy Source Shielding Experiment at the Los Alamos WNR Facility
Santa Fe Conference, May 13-17, 1985

/2/ P. Cloth, D. Filges, G. Sterzenbach, T.W. Armstrong, B.L. Colborn
The KFA-Version of the High-Energy Transport Code HETC and the generalized Evaluation Code SIMPEL
KFA-Report Jül-Spez-196, March 1983

/3/ W.W. Engle
ORNL-Report 1693, (1973)

/4/ J.T. Routti, J. Tapio
High-Energy Neutron Spectroscopy with Activation Detectors
UCRL-18514, 1969

/5/ KFA Report, to be published

/6/ W.B. Wilson
LA-7159-T, 1978

/7/ G. Rudstam
Zeitschriften für Naturforschung 21, 1027, 1966
see also: J.T. Routti, J.V. Sandberg
Computer Physics Communications
23, 411, 1981

/8/ M. Blann
Phys.Rev.Lett. 27, 337, 1971
and UCID 19614, 1982

/9/ R. Silberberg, C.H. Tsao
The Astrophysical Journal Supplement
Series No. 220 (I), 25, 315&335, 1973

/10/ C.J. Orth et al.
Journal of Inorganic Nuclear Chemistry 38, 13, 1976

/11/ A. Grütter
Nucl.Phys. A 383, 98, 1982

/12/ I.R. Williams, C.B. Fulmer
Phys.Rev. 162, 1055, 1967

/13/ L.R. Greenwood, R.K. Smither
DOE-ER-0046/14, 1983

ACKNOWLEDGEMENTS

The authors would like to thank Richard Woods and all other members of his group for their kind hospitality and continuous support.

Special thanks to the operators and other personnel associated with the WNR facility for their assistance with the irradiations.

Table I: Total Flux per cm^2 and per incident proton

Depth in Shield	Position in Fig. 5	HETC		HETC-ANISN coupling
		protons	neutron	neutrons
23 cm	A	6.38×10^{-9}	1.48×10^{-6}	1.85×10^{-6}
103 cm	B	0	1.70×10^{-8}	8.60×10^{-9}
203 cm	C	0	0	1.90×10^{-11}

Table II: Comparison of calculated and measured reaction rates

Cu-nat	Experiment	Rudstam		ALICE
	Run 1	HETC-ANISN coupling	HETC	HETC-ANISN coupling
		d = 23 cm		
Fe-59	2.1×10^{-33}	4.7×10^{-33}	3.5×10^{-33}	3.7×10^{-33}
Co-58	2.8×10^{-32}	4.5×10^{-32}	3.2×10^{-32}	9.3×10^{-32}
Co-57	1.4×10^{-32}	1.2×10^{-32}	0.8×10^{-32}	5.0×10^{-32}
Co-56	2.0×10^{-33}	2.4×10^{-33}	1.5×10^{-33}	16.0×10^{-33}
Mn-52	3.5×10^{-34}	6.3×10^{-34}	3.6×10^{-34}	60.0×10^{-34}
Mn-54	3.9×10^{-33}	5.3×10^{-33}	3.3×10^{-33}	14.0×10^{-33}
V-48	0.5×10^{-34}	1.0×10^{-34}	1.1×10^{-34}	20.0×10^{-34}
		d = 103 cm		
Fe-59	1.1×10^{-35}	2.7×10^{-35}	2.8×10^{-35}	1.8×10^{-35}
Co-58	1.8×10^{-34}	2.6×10^{-34}	2.5×10^{-34}	4.6×10^{-34}
Co-57	9.5×10^{-35}	7.5×10^{-35}	6.9×10^{-35}	27.0×10^{-35}
Co-56	1.7×10^{-35}	1.5×10^{-35}	1.3×10^{-35}	9.4×10^{-35}
Mn-52	2.8×10^{-36}	4.1×10^{-36}	3.2×10^{-36}	38.0×10^{-36}
Mn-54	3.2×10^{-35}	3.3×10^{-35}	2.8×10^{-35}	8.7×10^{-35}
V-48	1.0×10^{-36}	1.4×10^{-36}	0.9×10^{-36}	13.0×10^{-36}

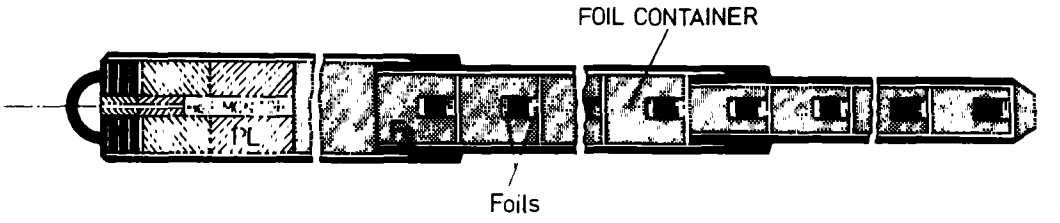

Fig. 1: The stringer assembly used to insert foil packages into the bulk shield of the WNR facility's Target I (LANSCE). Individual foil containers and foil positions are indicated. The ^{3}He monitor at the left is imbedded into PE rings and serves as a flux monitor.

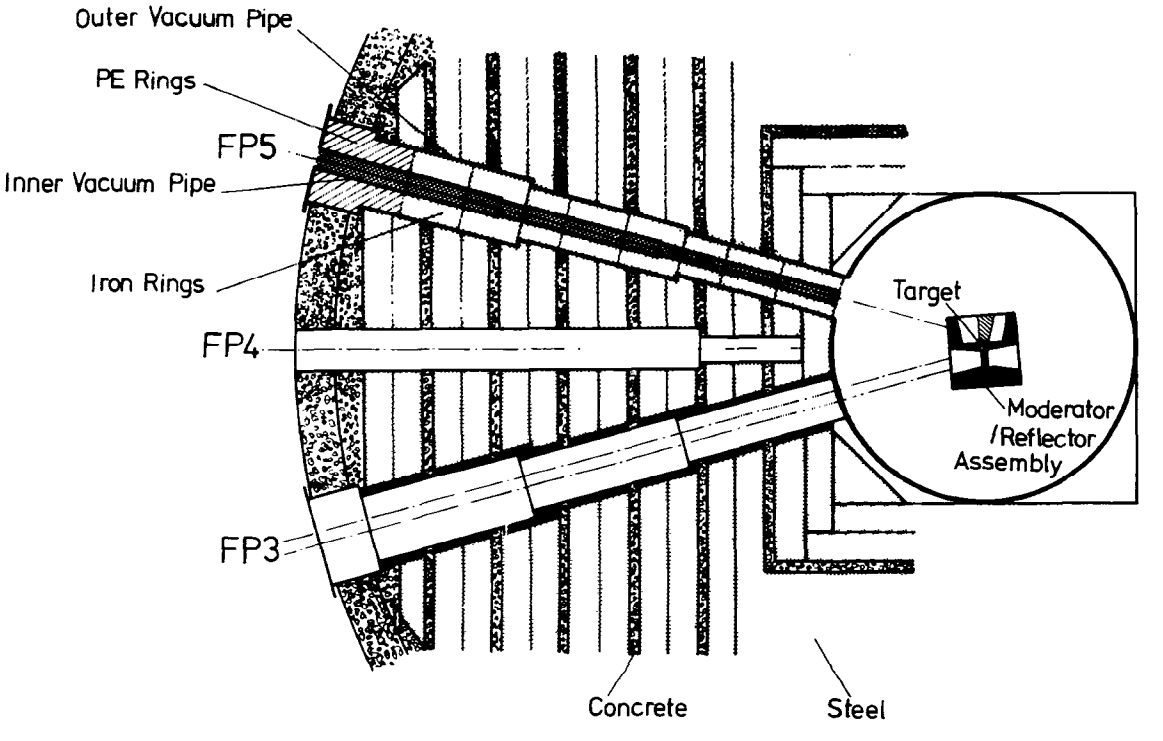

Fig. 2: Schematic scetch of the WNR target to the south. The stringer of Fig. 1 was inserted into Flight Path 5 (FP 5) for irradiations. Target, moderator and reflector are described in more detail in /5/

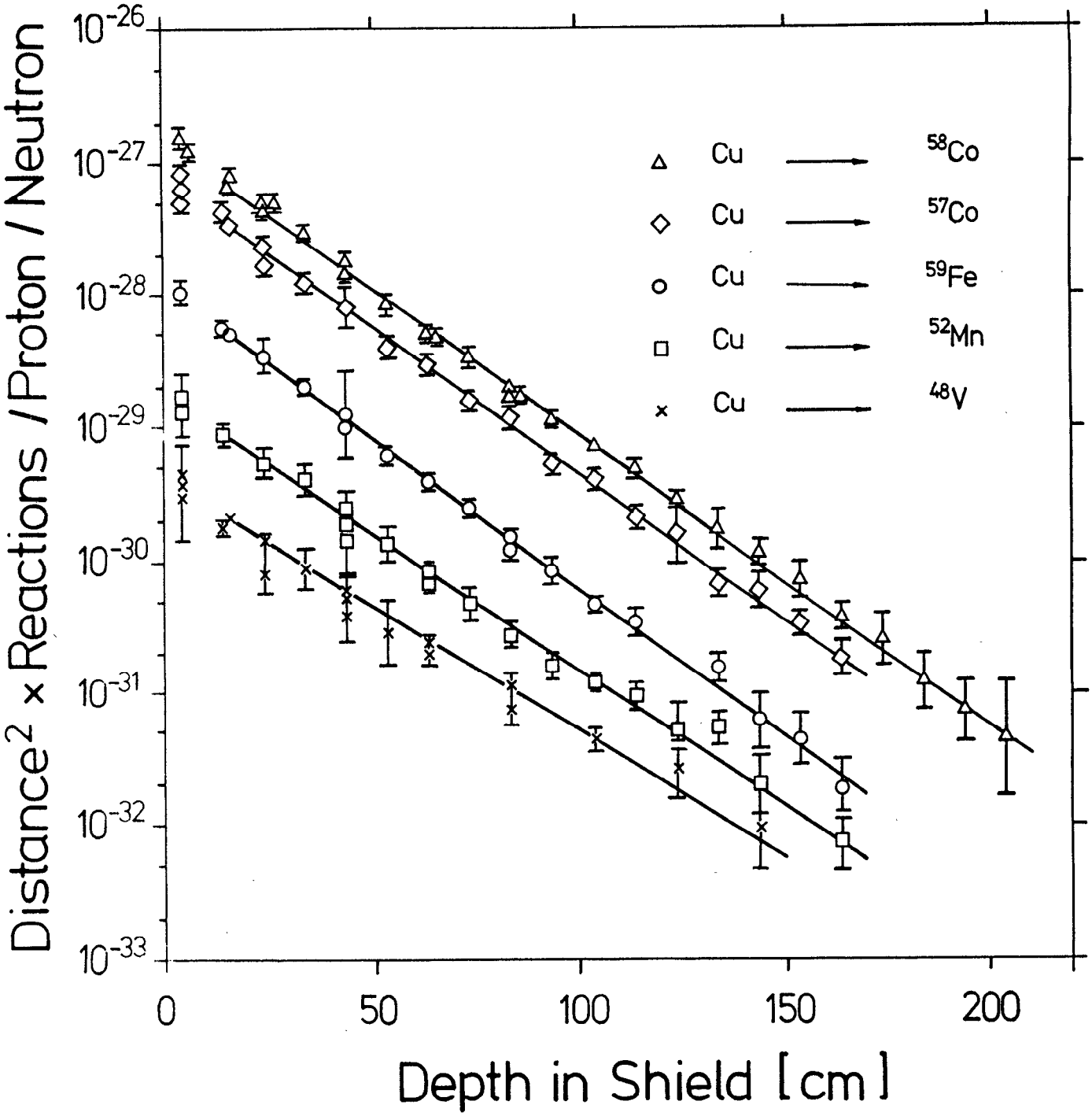

Fig. 3: Depth dependence of the reaction rates for some reactions on copper of natural isotopic composition. To eliminate solid angle dependence the reaction rates have been multiplied by the distance to the target center squared

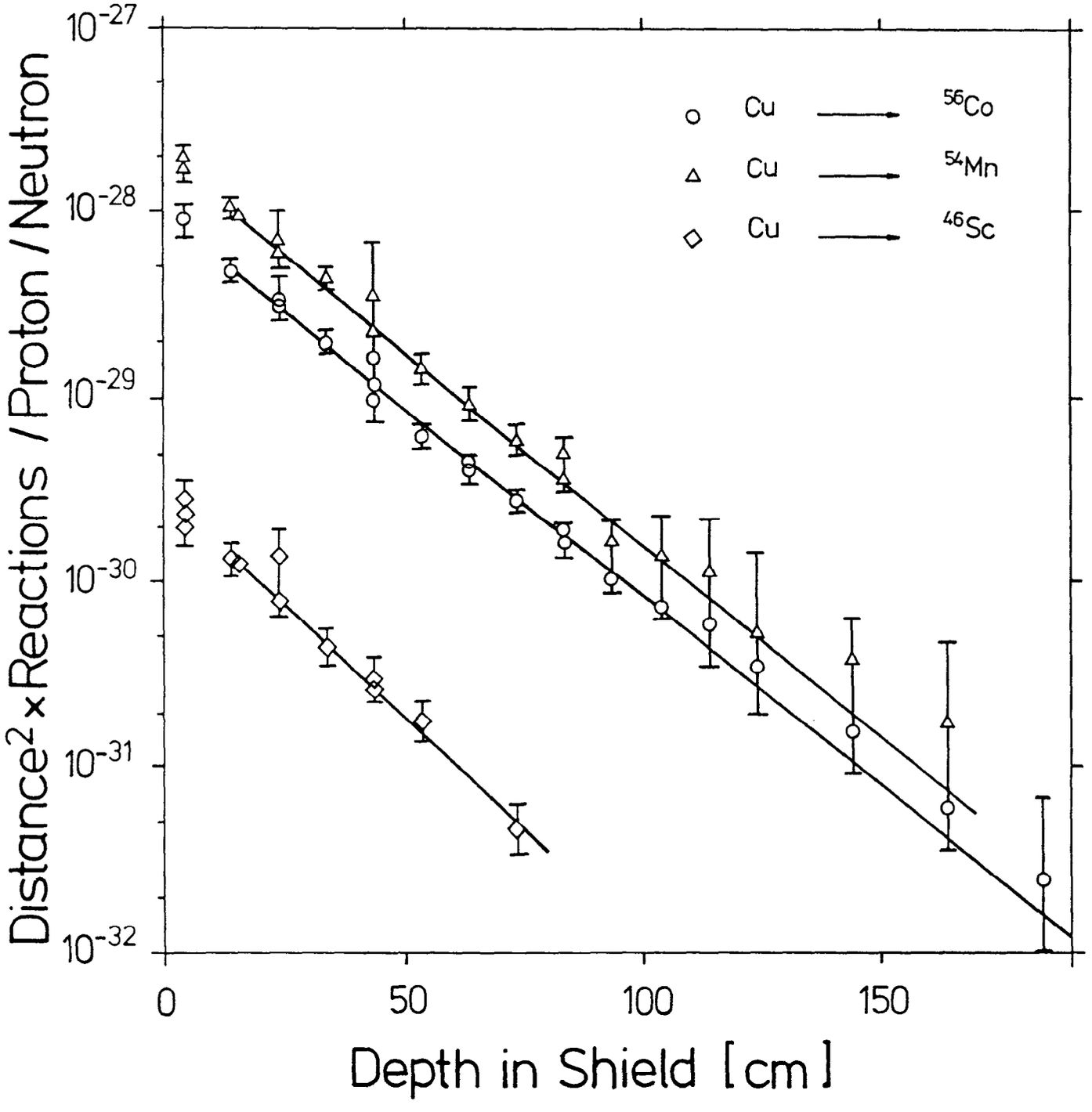

Fig. 4: Depth dependence of the reaction rates for some reactions on copper of natural isotopic compositions. To eliminate solid angle dependence the reaction rates have been multiplied by the distance to the target center squared

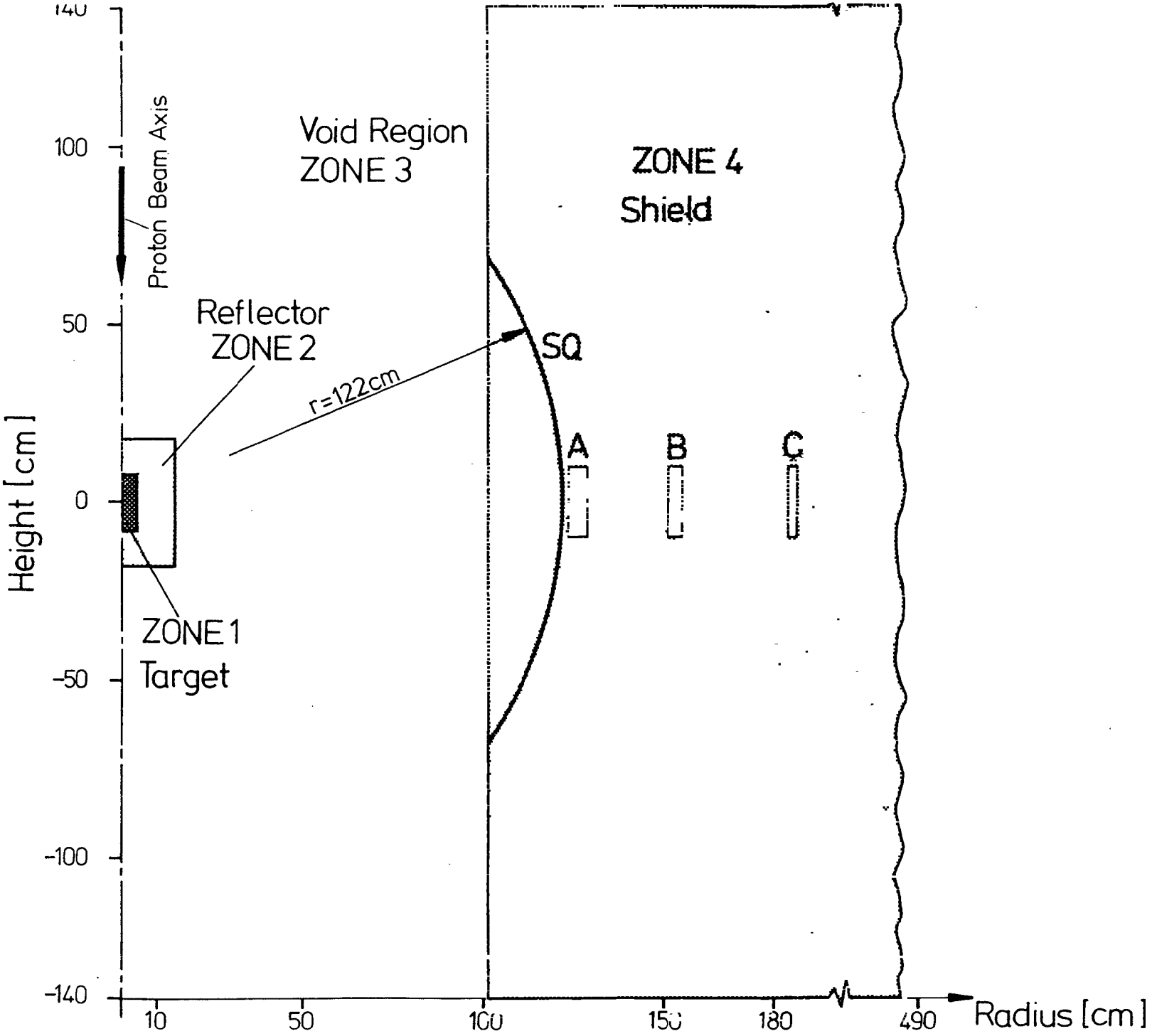

Fig. 5: Geometry

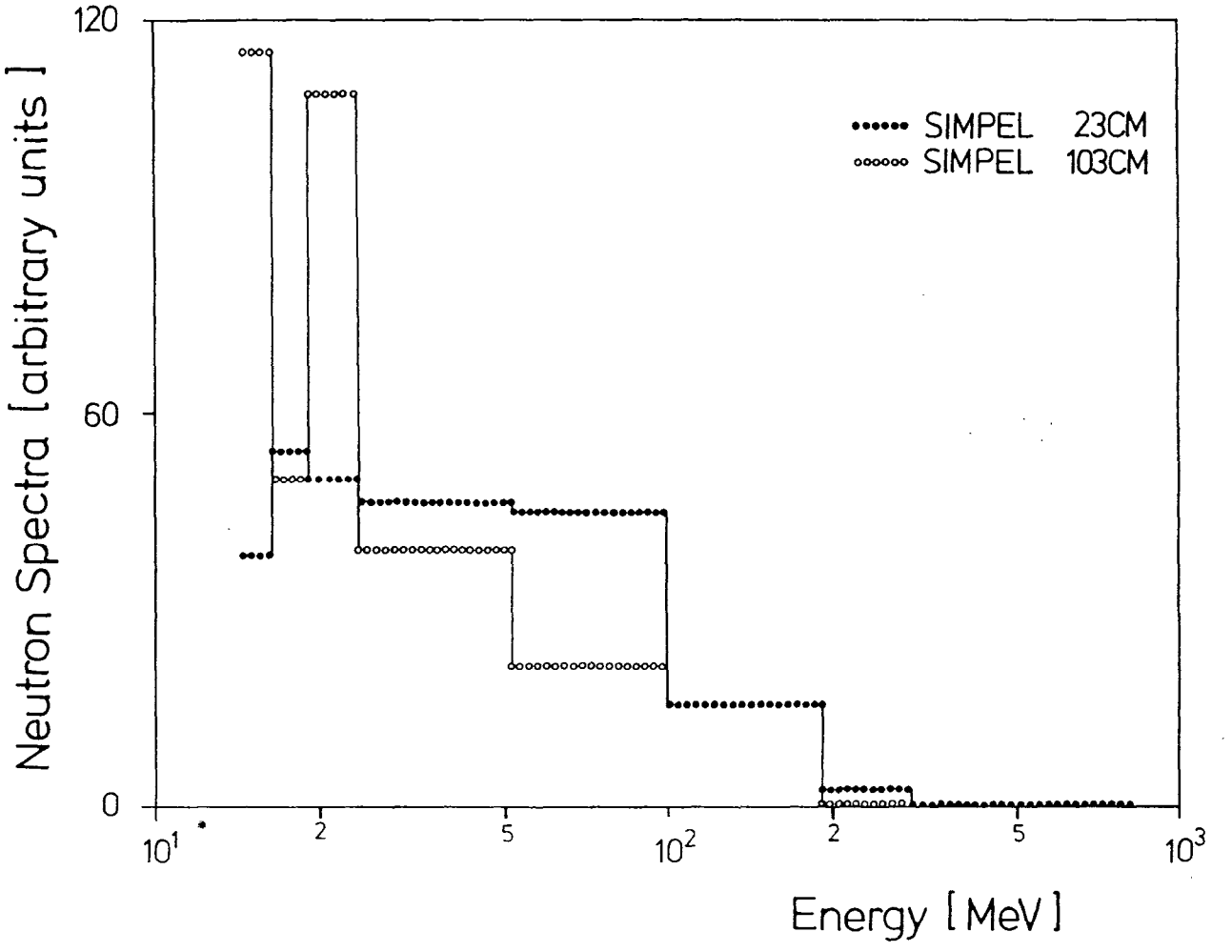

Fig. 6: HETC calculations

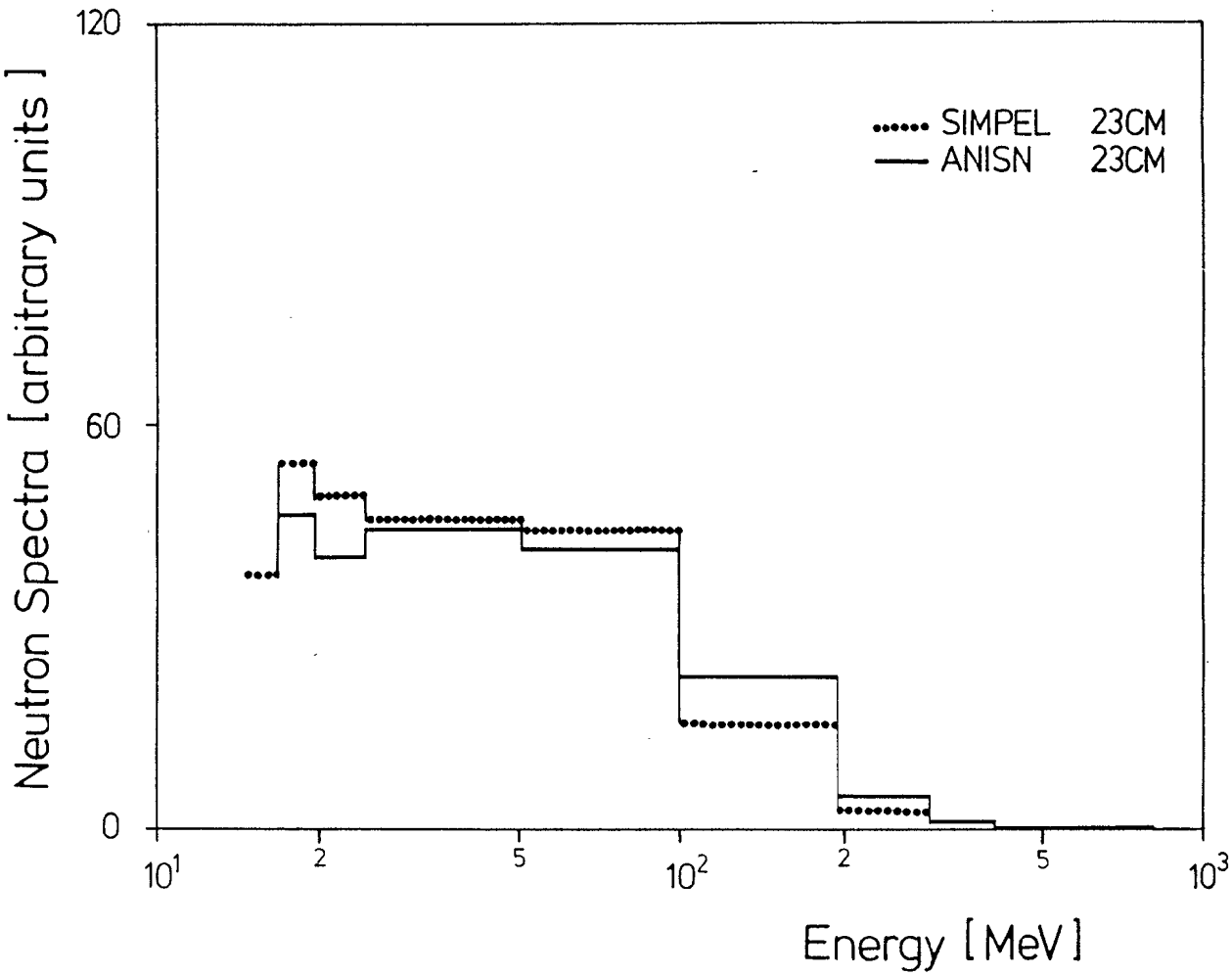

Fig. 7: Comparison of HETC-ANISN coupling and HETC calculations

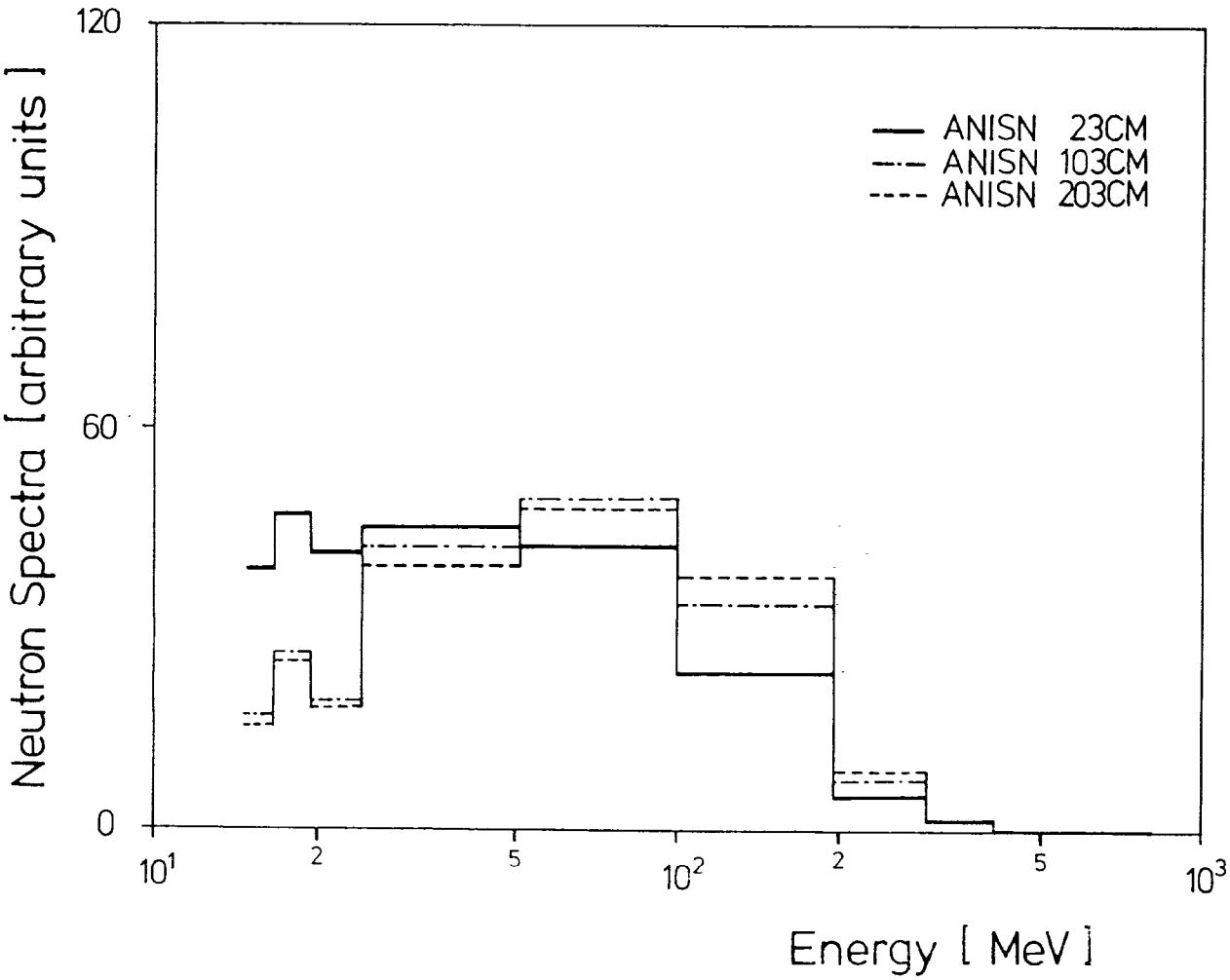

Fig. 8: HETC-ANISN coupling calculations

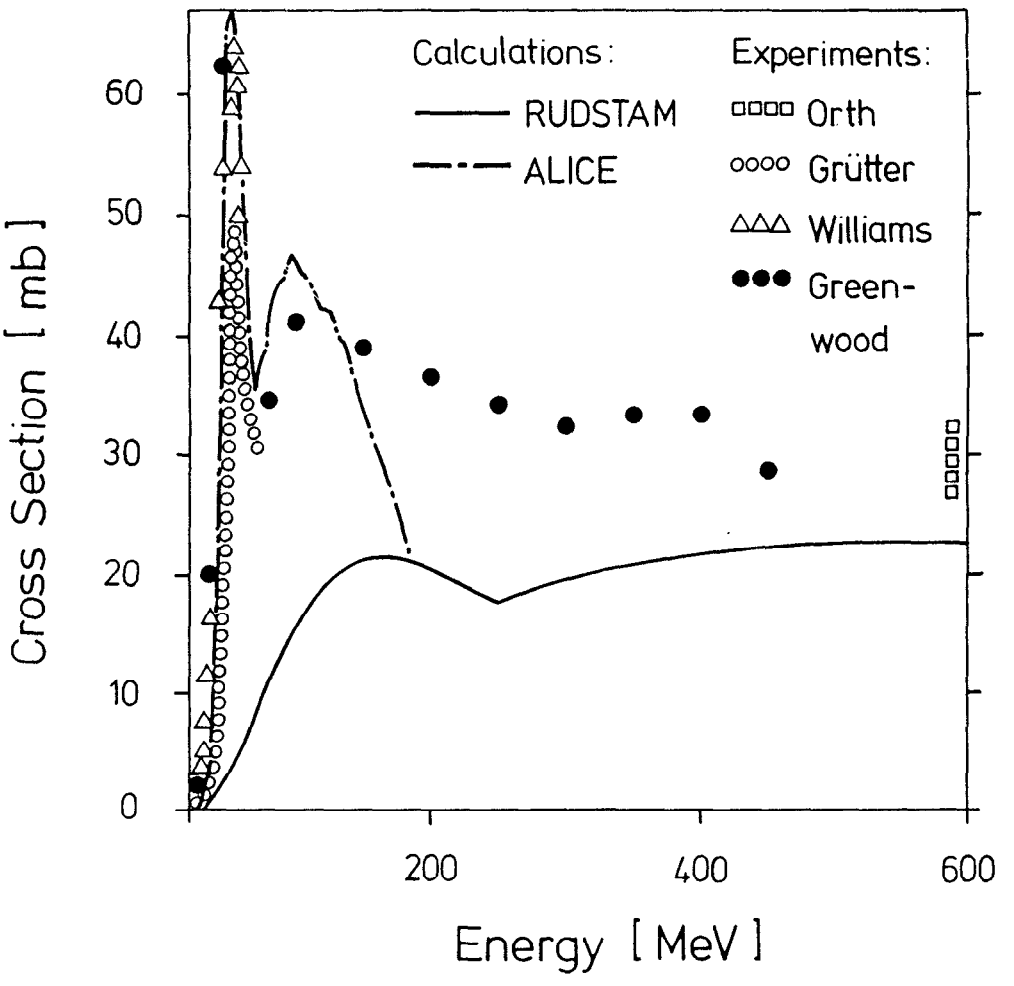

Fig. 9: Experimental cross sections /10-13/ and model calculations /7,8/ for the production of ^{57}Co from copper